NMR Pulse Schemes for the Sequence-Specific Assignment of Arginine Guanidino ^{15}N and ^{1}H Chemical Shifts in Proteins

Toshio Yamazaki,[†,‡] Steven M. Pascal,[†,‡] Alex U. Singer,[‡] Julie D. Forman-Kay,[‡] and Lewis E. Kay*,[†]

Contribution from the Protein Engineering Network Centres of Excellence and Departments of Medical Genetics, Biochemistry, and Chemistry, University of Toronto, Toronto, Ontario, Canada M5S 1A8, and Biochemistry Research Division, The Hospital for Sick Children, 555 University Avenue, Toronto, Ontario, Canada M5G 1X8

Received November 30, 1994[⊗]

Abstract: A family of 2D NMR experiments is presented for the sequence-specific assignment of arginine guanidino ^{1}H and ^{15}N chemical shifts based on the transfer of magnetization exclusively by scalar connectivities. Because of the potential for significant exchange with water at the ϵ and η positions along the side chain of arginine residues, care has been taken to minimize saturation and dephasing of water throughout the course of the pulse schemes. Attempts are made to minimize the effects of chemical exchange due to moderately slow rotation about the $N^{\epsilon}-C^{\zeta}$ bond of arginine. The methods are demonstrated on a 1.5 mM sample of the C-terminal SH2 domain from phospholipase-Cγ1 in complex with a 12-residue phosphotyrosyl peptide comprising its high-affinity binding site in the platelet-derived growth factor receptor.

Introduction

The past several years have witnessed a significant growth in the use of NMR spectroscopy to study protein structure and function.[1] Much of this growth is the result of the development of multidimensional, multinuclear NMR methods[2-8] which have extended the molecular weight limitations of the technique to the point where it is now quite feasible to study proteins or protein complexes with molecular weights on the order of 25 kDa. Methods exist, for example, for the facile assignment of backbone[2] ($^{1}H,^{15}N,^{13}C$) and side chain[9,10] ^{1}H and ^{13}C chemical shifts in uniformly $^{15}N,^{13}C$-labeled proteins which serve as the starting point for further structural or functional studies. Because of the importance of arginine side chain guanidino groups participating in stabilizing interactions in many protein-ligand complexes, including protein-DNA complexes[11,12] and Src homology 2 (SH2) signal transduction domains bound to phosphotyrosyl-containing peptides,[13-16] unambiguous assignment of these resonances is of considerable significance. It is often the case in such complexes that several of the arginine side chains are in spatial proximity leading to ambiguities in assignments based on NOEs. Recently Yamazaki et al. have developed experiments for correlating the arginine $H^{\epsilon},N^{\epsilon},C^{\zeta}$ chemical shifts via magnetization transfer employing scalar connectivities exclusively,[17] and Wittekind et al. have demonstrated that it is possible to observe $H^{\epsilon},N^{\epsilon},H^{\delta}$ correlations in the HNHA-gly experiment.[18] This work has been extended by Boelens, Kaptein, and co-workers in the development of a pulse scheme for establishing correlations between guanidino H^{ϵ},N^{η} chemical shifts.[19]

In this paper a family of pulse schemes is provided for the sequence-specific assignment of all arginine guanidino side chain ^{1}H and ^{15}N chemical shifts based on the transfer of magnetization via scalar couplings only. The method relies on knowledge of the assignments of the $^{1}H^{\delta}$ chemical shifts of each arginine, which are used to connect the guanidino group to its appropriate position in the primary sequence of the protein. Because the side chain guanidino protons are often quite labile, care has been taken to minimize saturation of water during the experiments. Moreover, the relatively slow rotation about the $N^{\epsilon}-C^{\zeta}$ bond results in a broadening of the line widths of the N^{η} and H^{η} spins. Care has been exercised in the design of pulse schemes to try to minimize the effect of the increased line widths of N^{η} spins, caused by the incomplete averaging of the chemical shift differences between the two η positions, on the quality of the resulting spectra. The approach is demonstrated on a 1.5 mM sample of the C-terminal SH2 domain of phospholipase-Cγ1 (PLCC SH2, 105 amino acids) in complex with a 12-residue phosphotyrosine-containing peptide (pY1021) comprising its high-affinity binding site on the platelet-derived growth factor receptor (PDGFR).

[†] University of Toronto.
[‡] The Hospital for Sick Children.
[⊗] Abstract published in *Advance ACS Abstracts,* March 1, 1995.

(1) Clore, G. M.; Gronenborn, A. M. *Science* **1991**, *252*, 1391.
(2) Bax, A.; Grzesiek, S. *Acc. Chem. Res.* **1993**, *26*, 131.
(3) Ikura, M.; Kay, L. E.; Bax, A. *Biochemistry* **1990**, *20*, 4569.
(4) Kay, L. E.; Ikura, M.; Tschudin, R.; Bax, A. *J. Magn. Reson.* **1990**, *89*, 496.
(5) Montelione, G.; Wagner, G. *J. Magn. Reson.* **1990**, *87*, 183.
(6) Clubb, R. T.; Thanabal, V.; Wagner, G. *J. Biomol. NMR* **1992**, *2*, 203.
(7) Wittekind, M. and Mueller, L. *J. Magn. Reson.* **1993**, *B101*, 201.
(8) Palmer, A. G.; Fairbrother, W. J.; Cavanagh, J.; Wright, P. E.; Rance, M. *J. Biomol. NMR* **1992**, *2*, 195.
(9) Kay, L. E.; Ikura, M.; Bax, A. *J. Am. Chem. Soc.* **1990**, *112*, 888.
(10) Bax, A.; Clore, G. M.; Gronenborn, A. M. *J. Magn. Reson.* **1990**, *88*, 425.
(11) Pavletich, N. P.; Pabo, C. O. *Science* **1991**, *252*, 809.
(12) Omichinski, J. G.; Clore, G. M.; Schaad, O.; Felsenfeld, G.; Trainor, C.; Appella, E.; Stahl, S. J.; Gronenborn, A. M. *Science* **1993**, *261*, 438.
(13) Waksman, G.; Shoelson, S. E.; Pant, N.; Cowburn, D.; Kuriyan, J. *Cell* **1993**, *72*, 779.
(14) Eck, M. J.; Shoelson, S. E.; Harrison, S. C. *Nature* **1993**, *362*, 87.
(15) Pascal, S. M.; Singer, A. U.; Gish, G.; Yamazaki, T.; Shoelson, S. E.; Pawson, T.; Kay, L. E.; Forman-Kay, J. D. *Cell* **1994**, *77*, 461.
(16) Lee, C. H.; Kominos, D.; Jacques, S.; Margolis, B.; Schlessinger, J.; Shoelson, S. E.; Kuriyan, J. *Structure* **1994**, *2*, 423.
(17) Yamazaki, T.; Yoshida, M.; Nagayama, K. *Biochemistry* **1993**, *32*, 5656.
(18) Wittekind, M.; Metzler, W. J.; Mueller, L. *J. Magn. Reson.* **1993**, *B101*, 214.
(19) Vis, H.; Boelens, R.; Mariani, M.; Stroop, R.; Vorgias, C. E.; Wilson, K. S.; Kaptein, R. *Biochemistry* **1994**, *33*, 14858.

0002-7863/95/1517-3556$09.00/0

Materials and Methods

A 1.5 mM sample consisting of a uniformly ^{15}N,^{13}C-labeled recombinant PLCC SH2 domain in complex with a 12-residue pY1021 phosphopeptide was prepared as described previously.[15] The sample was dissolved in 90% H_2O, 10% D_2O, and 0.1 M sodium phosphate, pH 6.3, at 30 °C.

All experiments were performed on a Varian UNITY-500 spectrometer equipped with a pulsed field gradient unit and a triple-resonance probe with an actively shielded z gradient. The Arg−$H^{\epsilon}(N^{\epsilon}C^{\delta})H^{\delta}$ experiment was recorded as a 64*512 complex matrix with spectral widths of 4 kHz (F_1) and 8 kHz (F_2), 1024 scans per FID, and a 1.15 s repetition rate to give a total recording time of 42 h. Both Arg−$H^{\epsilon}(N^{\epsilon}C^{\zeta})N^{\eta}$ and Arg−H^{η}-$(N^{\eta}C^{\zeta}N^{\epsilon})H^{\epsilon}$ experiments were recorded as 64*512 complex matrices, with 512 scans per FID and 1.15 s between scans to give total measuring times of 21 h/spectrum. F_1 spectral widths of 3.3 and 4.0 kHz were employed for the Arg−$H^{\epsilon}(N^{\epsilon}C^{\zeta})N^{\eta}$ and Arg−$H^{\eta}(N^{\eta}C^{\zeta}N^{\epsilon})H^{\epsilon}$ experiments, respectively, and an F_2 spectral width of 8 kHz was employed in both cases.

The activation energy for rotation about the $N^{\epsilon}-C^{\zeta}$ bond of arginine (~0.6 M unlabeled arginine from Sigma, dissolved in 70% H_2O, 10% D_2O, 20% methanol) was estimated from the temperature dependence of the rate constant describing the $N^{\epsilon}-C^{\zeta}$ rotation. Rate constants at −5, −10, −15, and −20 °C were determined using an HSQC pulse scheme with a delay T_m inserted between the t_1 evolution period and the final INEPT[20] transfer at the point where 2-spin order I_zN_z is created, as described in the literature.[21,22] (I_z and N_z are the z components of proton and nitrogen magnetization, respectively). This experiment gives rise to spectra with auto peaks ($N^{\eta i}$,$H^{\eta i}$) and cross peaks ($N^{\eta i}$,$H^{\eta j}$) ($i,j = \{1,2\}$, $i \neq j$), and the (assumed) 2-site jump rate between $\eta 1$ and $\eta 2$ can be estimated from the ratio of the auto and cross peak intensities as a function of T_m as described below. A number of small modifications were made to the original HSQC pulse scheme for measuring exchange. First, pulsed field gradients were included between the ^1H and ^{15}N 90° pulses during the transfer of magnetization from ^1H to ^{15}N and subsequent transfer from ^{15}N to ^1H to aid in the suppression of the intense water signal. In addition, a ^1H 90° pulse (of the same phase as the ^1H 90° pulse in the final INEPT[20] transfer) was inserted immediately prior to detection to (i) aid in the elimination of signal from protons one-bond coupled to ^{14}N nuclei and to (ii) eliminate dispersive contributions to the H^{η} line shape in F_2 caused by exchange between $\eta 1$ and $\eta 2$ during the INEPT transfer from ^{15}N to ^1H. The values of T_m used for the various temperatures are as follows: T_m = 1, 6, 10 ms (−5 °C); T_m = 1, 6, 11, 16, 21 ms (−10 °C); T_m = 1, 6, 11, 16, 21 ms (−15 °C); T_m = 1, 11, 21, 31 ms (−20 °C). 2D exchange spectra were recorded as 128*512 complex matrices with 16 scans per FID and a relaxation delay of 1.0 s between scans. It is straightforward to show that, (i) neglecting $^1H-^1H$ cross relaxation and (ii) assuming that the rotation about the $N^{\epsilon}-C^{\zeta}$ bond of arginine can be characterized by a 2-site jump with each site having identical relaxation properties, the time dependence of cross and auto peaks, $I_c(T_m)$ and $I_a(T_m)$, respectively, are given by $I_c(T_m) = 0.5I_a(0)\exp(-\varrho T_m)\{1 - \exp(-2kT_m)\}$ and $I_a(T_m) = 0.5I_a(0)\exp(-\varrho T_m)\{1 + \exp(-2kT_m)\}$, where k is the jump rate, and ϱ is the decay rate of 2-spin order I_zN_z and includes the effects of exchange with water. The value of k can be extracted from the ratio $[I_a(T_m) - I_c(T_m)]/[I_a(T_m) + I_c(T_m)]$, which is independent of ϱ. Values of the activation energy for the 2-site jump were calculated from the temperature dependence of k according to the Arrhenius equation, $k = A\exp(-E_a/RT)$, where A is the frequency factor, E_a is the activation energy, T is the absolute temperature, and $R = 8.314$ J mol^{-1} K^{-1}.

Results and Discussion

Our interest in developing methods for the sequence-specific assignment of arginine (N^{ϵ},H^{ϵ}) and (N^{η},H^{η}) chemical shifts was stimulated by structural studies of a complex of the PLCC SH2 domain with the 12-residue pY1021 phosphopeptide. Our recent solution structure of the complex[15] shows that four of the nine arginine side chain guanidino groups are in the phosphotyrosine binding pocket and can potentially interact with the phosphate group of the peptide. Sequence alignment of PLCC, Src, and Lck SH2 domains indicates that only two of the four arginines found in the phosphotyrosine binding pocket of the PLCC SH2 are conserved in Src and Lck, with a lysine substituted for one of the other arginines (see Figure 1 of ref 15). The additional positively charged side chain in proximity to the phosphotyrosine in the PLCC SH2 domain relative to Src or Lck SH2 domains suggests that not all of the four arginines may be equally important in binding. That this is the case is illustrated in Figure 1, which shows a portion of the $^1H-^{15}N$ HSQC spectrum of the PLCC SH2−pY1021 complex. Note that two of the (N^{η},H^{η}) cross peaks are shifted significantly downfield relative to the remaining NH_2 cross peaks in both ^{15}N and ^1H dimensions (Arg 37) and that one of the nine (N^{ϵ},H^{ϵ}) cross peaks, in particular, is shifted appreciably upfield in the ^{15}N dimension (Arg 37). These anomalously shifted cross peaks are not observed in the case of the uncomplexed PLCC SH2 domain in non-phosphate buffers.[23] The recognition that the chemical shift differences observed in the spectrum may provide important insight into the different roles of the arginines in the phosphotyrosine binding site has led to the development of methods for their sequential assignment. The use of NOEs for assignment of these resonances can be ambiguous, especially given the presence of four arginine side chains within the phosphotyrosine binding site. Moreover, rapid exchange with solvent results in the attenuation of many of the NOEs from H^{η} or H^{ϵ} protons, further complicating NOE-based assignment strategies. Because NOEs connecting the arginine side chains to the phosphotyrosine of the peptide are sparse, knowledge of the chemical shifts could potentially provide structural information through the use of chemical shift refinement methods.[24] Additionally, the assignment of the chemical shifts serves as the starting point for detailed studies of arginine side chain dynamics and hydrogen exchange properties.

Figure 2 illustrates the pulse schemes that were developed for the sequence-specific assignment of (N,H) cross peaks of arginine guanidino side chains using methods based exclusively on scalar connectivities. The three pulse schemes that we have used in the present study are described below. While the first two sequences are similar to experiments already in the literature,[17-19] particular emphasis in the design of the present experiments has been placed on optimizing sensitivity which has proven crucial in the application to the SH2−pY1021 complex.

(1) Arg−$H^{\epsilon}(N^{\epsilon}C^{\delta})H^{\delta}$ (Figure 2a). The flow of magnetization in this experiment can be described succinctly as follows:

$$H^{\epsilon} \xrightarrow{J_{NH}} N^{\epsilon} \xrightarrow{J_{N^{\epsilon}C^{\delta}}} C^{\delta} \xrightarrow{J_{CH}} H^{\delta}(t_1) \xrightarrow{J_{CH}} C^{\delta} \xrightarrow{J_{N^{\epsilon}C^{\delta}}} N^{\epsilon} \xrightarrow{J_{NH}} H^{\epsilon}(t_2) \quad (1)$$

(20) Morris, G. A.; Freeman, R. *J. Am. Chem. Soc.* **1979**, *101*, 760.
(21) Wider, G.; Neri, D.; Wuthrich, K. *J. Biomol. NMR* **1991**, *1*, 93.
(22) Otting, G.; Liepinsh, E.; Wuthrich, K. *Biochemistry* **1993**, *32*, 3571.
(23) Pascal, S. M.; Yamazaki, T.; Singer, A. U.; Kay, L. E.; Forman-Kay, J. D. In preparation.
(24) Harvey, T. S.; van Gunsteren, W. F. *Techniques in Protein Chemistry*; Angeletti, R. H., Ed.; Academic Press: New York, 1993; 615.

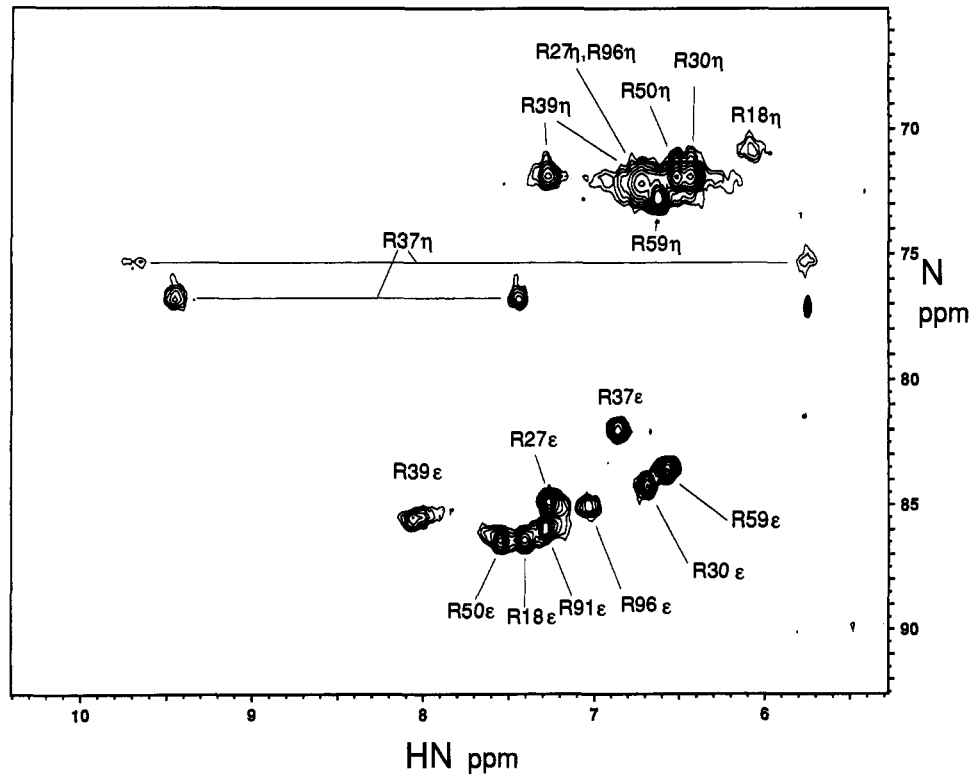

Figure 1. A portion of the 2D $^1H-^{15}N$ HSQC spectrum of the PLCC SH2 domain bound to a 12-residue phosphotyrosine peptide from the platelet-derived growth factor receptor showing the arginine side chain resonances. Assignments were made using the experiments described in the text and are summarized in Table 1.

with the scalar couplings active during each magnetization transfer step listed above the arrows. The design of the pulse scheme is based on the "out and back" approach[4] discussed previously in the literature and is similar to the HNHA−gly[18] and HNCAHA pulse schemes[25] which correlate (H^α,^{15}N,HN) chemical shifts. The 2D data set generated from the present sequence, after Fourier transformation, gives rise to cross peaks at (ω_{H^δ},ω_{H^ϵ}), and comparison of the H^δ chemical shift(s) obtained from this experiment with the H^δ shift(s) determined previously using carbon−carbon TOCSY/COSY-based experiments[9,10,26-28] provides the sequence-specific assignment of the H^ϵ shifts. Once the H^ϵ shifts are assigned, the N^ϵ shifts can be readily deduced from an HSQC spectrum. Alternatively, it is possible to record a 3D spectrum which correlates N^ϵ, H^ϵ, and H^δ directly; however, this approach was not taken in the present study.

While the magnetization transfer steps employed in the present pulse scheme are straightforward and similar to the transfer in the HNHA−gly sequence,[18] a number of aspects of this experiment are worthy of comment. First, in order to ensure that only cross peaks of the type (ω_{H^δ},ω_{H^ϵ}) are obtained and not the backbone peaks resonating at (ω_{H^α},ω_{H^N}), selective ^{15}N 180° pulses have been inserted in both the initial and final INEPT[20] transfers in the sequence and are denoted by the shaped nitrogen pulses in Figure 2a. (The chemical shifts of the $^{15}N^\epsilon$ and backbone ^{15}N spins are 80−90 ppm and 100−135 ppm, respectively.) By insuring that the bandwidth of these pulses does not include the backbone ^{15}N spins, the corresponding pathway to that described in eq 1 for backbone nuclei cannot occur.

Second, as described in the introduction, it is crucial for the optimum sensitivity of these experiments that saturation of water magnetization be minimized and that the water magnetization be restored to the $+z$ axis prior to detection.[29-31] To this end, the sequence makes use of water selective pulses denoted by the shaped ^1H pulses in Figure 2a, and care is taken in the design of the phase cycling. After the first water-selective pulse (point a in the sequence) the water magnetization is restored to the $+z$ axis. At the conclusion of the subsequent τ_b period, during which antiphase ^{15}N magnetization refocuses, ^1H decoupling commences to maintain inphase nitrogen magnetization. Note that the ^1H $90°_y$ pulse at the start of the period rotates the water magnetization so that it is aligned with the ^1H decoupling field (decoupling pulses applied along the $\pm x$ axes) and therefore is unaffected by the ^1H pulses.[31] The long $T_{1\rho}$ of water ensures that essentially no decay occurs during this period, and water magnetization is restored to the $+z$ axis at the conclusion of decoupling by the action of the $90°_{-y}$ pulse. Note that the ^1H $90°_{\pm y}$ flanking pulses are not necessary if an integral number of WALTZ-16_x[32] decoupling cycles are employed; however, this requires careful attention to the lengths of the τ_c delays and the ^1H, ^{15}N, and $^{13}C^\delta$ pulse widths, and for this reason we prefer the approach illustrated in Figure 2. The subsequent three ^1H pulses (between points b and c in the Figure 2) rotate the water magnetization 360° and hence restore the water to the $+z$ axis.

(25) Kay, L. E.; Wittekind, M.; McCoy, M. A.; Friedrichs, M. S.; Mueller, L. *J. Magn. Reson.* **1992**, *98*, 443.
(26) Grzesiek, S.; Anglister, J.; Bax, A. *J. Magn. Reson.* **1994**, *B101*, 114.
(27) Logan, T. M.; Olejniczak, E. T.; Xu, E. T.; Fesik, S. W. *FEBS Lett.* **1992**, *314*, 413.
(28) Montelione, G. T.; Lyons, B. A.; Emerson, S. D.; Jashiro, M. *J. Am. Chem. Soc.* **1992**, *114*, 10974.
(29) Grzesiek, S.; Bax, A. *J. Chem. Soc.* **1993**, *115*, 12593.
(30) Stonehouse, J.; Shaw, G. L.; Keeler, J.; Laue, E. *J. Magn. Reson.* **1994**, *A107*, 178.
(31) Kay, L. E.; Xu, G. Y.; Yamazaki, T. *J. Magn. Reson.* **1994**, *A109*, 129.
(32) Shaka, A. J.; Keeler, J.; Frenkiel, T.; Freeman, R. *J. Magn. Reson.* **1983**, *52*, 335.

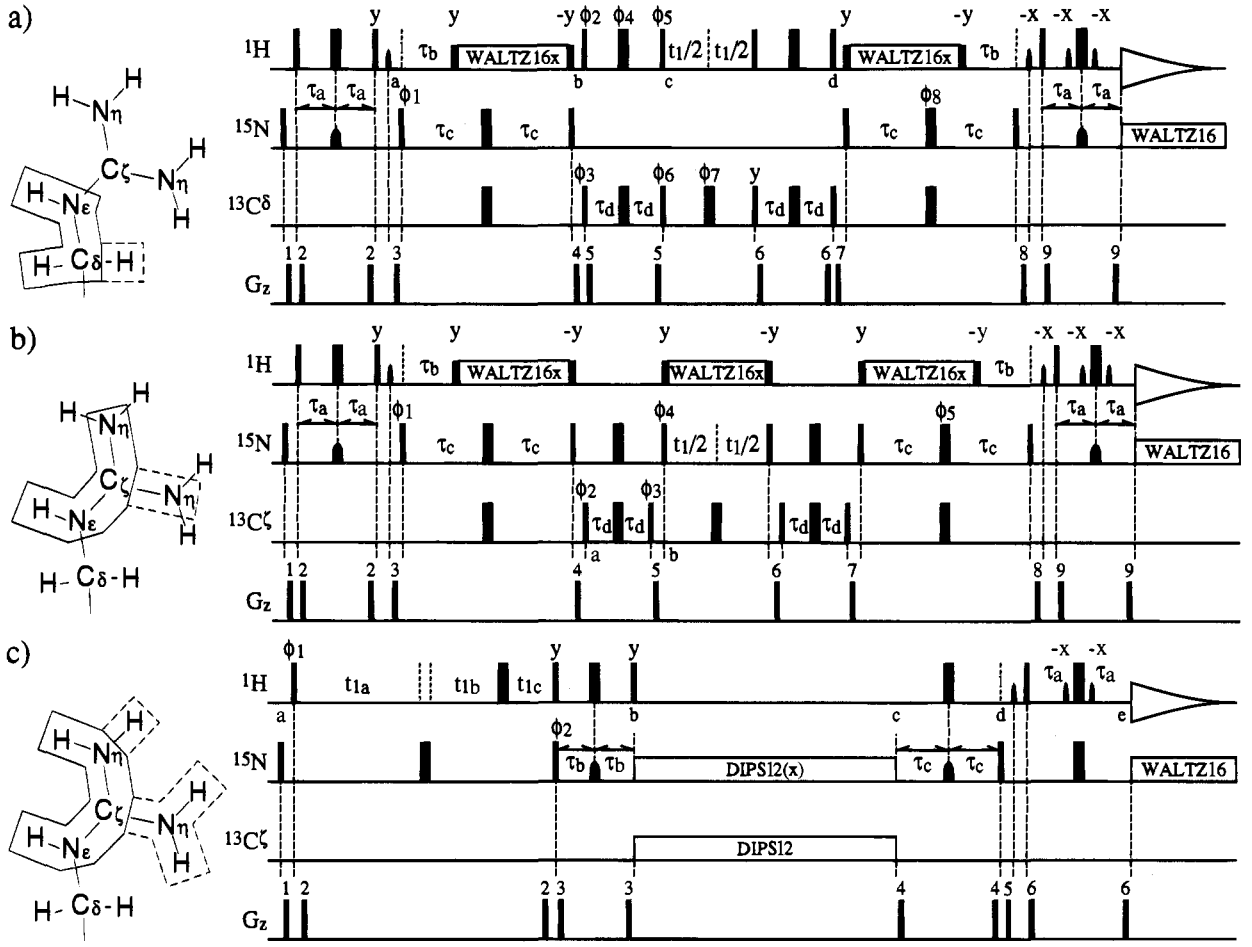

Figure 2. Pulse sequences for the assignment of the arginine guanidino ^{15}N and ^{1}H chemical shifts. The schematic to the left of each sequence indicates the spins involved in each magnetization transfer pathway. (a) Pulse scheme of the Arg−$H^{\epsilon}(N^{\epsilon}C^{\delta})H^{\delta}$ experiment. All narrow (wide) rectangular pulses have a flip angle of 90° (180°). All proton pulses are centered on the water resonance and are applied with a field of 24 kHz with the following exceptions: the water-selective pulses (denoted by the shaped ^{1}H pulses) immediately preceding gradient g_3 and after g_8 are applied as 2.7 ms (200 Hz at peak height) pulses having the profile of a 90° SEDUCE-1[37] element; the final two water-selective pulses, flanked by gradients g_9, are applied as 1.5 ms rectangular pulses; the ^{1}H 90°$_y$ pulses flanking the WALTZ-16$_x$[32] (all pulses along $\pm x$ axes) decoupling periods are applied with a 6.25 kHz field as are the ^{1}H WALTZ[32] decoupling fields. The ^{15}N pulses are centered at 85 ppm, and the pulses denoted by rectangles are applied with a 5.3 kHz rf field. The first shaped ^{15}N pulse has a duration of 1.4 ms and a SEDUCE-1[37] profile (780 Hz at peak height). The final ^{15}N pulse is applied as a 0.5 ms rectangular pulse. ^{15}N-decoupling during acquisition is achieved with a 1.0 kHz WALTZ[32] decoupling field. All $^{13}C^{\delta}$ pulses are applied with the carbon carrier centered at 43 ppm using an rf field of 8.3 kHz. The use of this field minimizes excitation of the $^{13}C^{\zeta}$ spins (centered at ~158 ppm[17]) by the $^{13}C^{\delta}$ 180° pulses, thereby ensuring that the transfer of magnetization proceeds between $^{15}N \leftrightarrow {}^{13}C^{\delta}$ and not $^{15}N \leftrightarrow {}^{13}C^{\zeta}$ during the INEPT[20] transfers. The delays used in the sequence are $\tau_a = 2.4$ ms, $\tau_b = 5.5$ ms, $\tau_c = 18.0$ ms, and $\tau_d = 0.8$ ms. Numerical simulations (verified by experiment) show that during the initial and final INEPT[20] periods of duration $2\tau_a$, evolution due to the $^{1}H-^{15}N$ scalar coupling proceeds during the application of the (long) ^{15}N 180° pulse of duration pw_N for an effective time, $\tau = (2/\pi)\ pw_N$ in the case of a rectangular nitrogen pulse and for an effective time, $\tau = (0.82)pw_N$ in the case of a pulse having the SEDUCE-1[37] profile. Therefore the effective time for the evolution of $^{1}H-^{15}N$ scalar coupling is 4.5 ms for the first INEPT period and 4.6 ms for the second. The phase cycle employed is as follows: $\phi_1 = (x,-x)$; $\phi_2 = 4(x),4(-x)$; $\phi_3 = 2(x),2(-x)$; $\phi_4 = \mathbf{4}(x)$, $4(-x)$; $\phi_5 = 4(x),4(-x)$; $\phi_6 = 8(y),8(-y)$; $\phi_7 = 16(x),16(-x)$; $\phi_8 = 32(x),32(-x)$; rec = $x,2(-x),x,2\{-x,2(x),-x\},x,2(-x),x$. The delays and strengths of the gradients are as follows: $g_1 = (0.5$ ms, 8 G/cm), $g_2 = (0.5$ ms, 4 G/cm), $g_3 = (1.0$ ms, 10 G/cm), $g_4 = (0.5$ ms, 12 G/cm), g_5 (0.1 ms, 15 G/cm), $g_6 = (0.2$ ms, 10 G/cm), $g_7 = (0.8$ ms, 10 G/cm), $g_8 = (1.0$ ms, 12 G/cm), $g_9 = (0.2$ ms, 8 G/cm). Quadrature in F_1 is obtained by incrementing the phases of ϕ_2, ϕ_4, and ϕ_5 simultaneously by 90°.[38] (b) Pulse scheme of the Arg−$H^{\epsilon}(N^{\epsilon}C^{\zeta})N^{\eta}$ experiment. Details concerning the strength of the rf fields employed and the durations and shapes of pulses are as described in (a) with the exception that the carbon carrier is placed in the center of the $^{13}C^{\zeta}$ region of the carbon spectrum, 158 ppm. The delays used in the sequence are $\tau_a = 2.4$ ms, $\tau_b = 5.5$ ms, $\tau_c = 11.0$ ms, and $\tau_d = 7.0$ ms. The phase cycle employed is as follows: $\phi_1 = (x,-x)$; $\phi_2 = 2(x),2(-x)$; $\phi_3 = 4(x),4(-x)$; $\phi_4 = 8(x),8(-x)$; $\phi_5 = 16(x),16(-x)$; rec = $x,2(-x),x,2\{-x,2(x),-x\},x,2(-x),x$. The delays and strengths of the gradients are $g_1 = (0.5$ ms, 8 G/cm), $g_2 = (0.5$ ms, 5 G/cm), $g_3 = (1.0$ ms, 15 G/cm), $g_4 = (0.75$ ms, 20 G/cm), $g_5 = (1.0$ ms, 6 G/cm), $g_6 = (1.0$ ms, 4 G/cm), $g_7 = (0.2$ ms, 5 G/cm), $g_8 = (1.0$ ms, 12 G/cm), and $g_9 = (0.2$ ms, 20 G/cm). Quadrature in F_1 is obtained by incrementing the phase of ϕ_4 using the States−TPPI[39] method. (c) Pulse scheme of the Arg−$H^{\eta}(N^{\eta}C^{\zeta}N^{\epsilon})H^{\epsilon}$ experiment. ^{1}H pulse widths and pulse shapes are as described in (a). Details concerning ^{15}N pulses are as in (a) with the exceptions that the carrier is placed at 79 ppm and that the shaped 180° pulses are applied as 1 ms (1.1 kHz at peak height) SEDUCE[37] pulses. $^{15}N-^{13}C$ heteronuclear cross-polarization is accomplished using a 0.9 kHz DIPSI-2[40] mixing scheme applied simultaneously to both ^{15}N and ^{13}C spins for 64 ms. The carbon carrier is at 158 ppm. The delays used in the sequence are $\tau_a = 2.3$ ms, $\tau_b = 1.45$ ms, $\tau_c = 2.81$ ms, $t_{1a} = t_1/2 + \tau_a$, $t_{1b} = t_1/2 - n\zeta$, and $t_{1c} = \tau_a - n\zeta + 2{*}pw_N$, where $\zeta = (\tau_a - g_2 + 2{*}pw_N)/(N-1)$, $n = 0, 1, 2 \ldots N\text{-}1$, N is the number of complex acquisition points in the t_1 dimension, pw_N is the ^{15}N 90° pulse width, and g_2 is the duration of the second pulsed field gradient, indicated by the number "2" in the figure.[41,42] The phase cycle employed is as follows: $\phi_1 = (x,-x)$; $\phi_2 = 2(x),2(-x)$; rec = $(x,-x,-x,x)$. The delays and strengths of the gradients are $g_1 = (0.6$ ms, 8 G/cm), $g_2 = (0.2$ ms, 10 G/cm), $g_3 = (0.5$ ms, 9 G/cm), $g_4 = (0.25$ ms, 4 G/cm), $g_5 = (2.0$ ms, 10 G/cm), and $g_6 = (0.2$ ms, 15 G/cm). Quadrature in F_1 is obtained by incrementing the phase of ϕ_1 using the method of States.[38]

Note that the phases of the three pulses, ϕ_2, ϕ_4, and ϕ_5, are incremented by 90° simultaneously to record the quadrature component of magnetization in the indirectly detected dimension. At first glance it may seem that the ^{1}H 90° pulse of phase ϕ_2 is unnecessary. Indeed, it serves no purpose insofar as magnetization transfer is concerned, and at point b in the sequence there is no proton magnetization associated with the protein that will give rise to a signal of interest. Furthermore, for the cosine t_1-modulated component of the signal, it is possible to eliminate this pulse and, by the careful choice of phases of other ^{1}H pulses in the sequence, ensure that water magnetization is placed along the $+z$ axis by the detection period. However, it is not clear how the same result can be achieved for the sine t_1-modulated component without the insertion of additional pulses. The approach taken here, where a ^{1}H pulse of phase ϕ_2 is included in the scheme, ensures that, for both quadrature components of magnetization, the water magnetization is positioned along the $+z$ axis at the conclusion of the sequence and that water magnetization is preserved with the same intensity for both x and y components of the t_1 signal. This is important since, if the steady state water signal is different for the x and y components, exchange with labile protons, such as the H^ϵ proton, can give rise to F_1 quadrature artifacts for cross peaks involving these protons. Note also that, in a manner similar to the ^{1}H pulse of phase ϕ_2, the ^{1}H 90° pulse applied at point d in the sequence has no affect insofar as the magnetization transfer pathway is concerned, but serves to place the water magnetization on the $+z$ axis prior to the application of gradient g_7.

(2) Arg−H$^\epsilon$(N$^\epsilon$C$^\zeta$)N$^\eta$ (Figure 2b). The flow of magnetization in this experiment is shown in eq 2 with the appropriate scalar couplings indicated above the arrows. This experiment

$$H^\epsilon \xrightarrow{J_{NH}} N^\epsilon \xrightarrow{J_{N\epsilon C\zeta}} C^\zeta \xrightarrow{J_{N\eta C\zeta}} N^\eta(t_1) \xrightarrow{J_{N\eta C\zeta}} C^\zeta \xrightarrow{J_{N\epsilon C\zeta}} N^\epsilon \xrightarrow{J_{NH}} H^\epsilon(t_2) \quad (2)$$

provides sequence-specific assignments of the N^η resonances from a knowledge of the H^ϵ chemical shifts obtained from the H$^\epsilon$(N$^\epsilon$C$^\delta$)H$^\delta$ experiment described above. With minor modifications to this scheme it is possible to record the C^ζ chemical shift as well; however, because of the near degeneracy of many of the C^ζ shifts, we have not found this to be useful. Recently, Vis et al. have proposed a similar experiment and applied it in their structural studies of the 19.5 kDa DNA binding protein, HUBst.[19]

Many of the same considerations necessary to insure the optimal performance of the Arg−H$^\epsilon$(N$^\epsilon$C$^\delta$)H$^\delta$ sequence were also important in the design of the present experiment and will not be reiterated. At point a in Figure 2b the magnetization of interest is given by the operator $2N^\epsilon{}_zC^\zeta{}_y$, where $N^\epsilon{}_z$ and $C^\zeta{}_y$ denote the z and y components of magnetization associated with the N^ϵ and C^ζ spins, respectively. During the subsequent period $2\tau_d$ this operator evolves to give the following terms: $2N^\epsilon{}_zC^\zeta{}_y \cos^3(2\pi J\tau_d)$; $2N^{\eta1}{}_zC^\zeta{}_y \cos(2\pi J\tau_d) \sin^2(2\pi J\tau_d)$; $2N^{\eta2}{}_zC^\zeta{}_y \cos(2\pi J\tau_d) \sin^2(2\pi J\tau_d)$; $8N^\epsilon{}_zC^\zeta{}_yN^{\eta1}{}_zN^{\eta2}{}_z \cos(2\pi J\tau_d) \sin^2(2\pi J\tau_d)$; $C^\zeta{}_x \cos^2(2\pi J\tau_d) \sin(2\pi J\tau_d)$; $4N^\epsilon{}_zC^\zeta{}_xN^{\eta1}{}_z \cos^2(2\pi J\tau_d) \sin(2\pi J\tau_d)$; $4N^\epsilon{}_zC^\zeta{}_xN^{\eta2}{}_z \cos^2(2\pi J\tau_d) \sin(2\pi J\tau_d)$; and $4C^\zeta{}_xN^{\eta1}{}_zN^{\eta2}{}_z \sin^3(2\pi J\tau_d)$, where J is the coupling between the C^ζ carbon and any of the N^ϵ, $N^{\eta1}$, and $N^{\eta2}$ nitrogens (assumed equal[33]). The last four terms are eliminated by the phase cycling of ϕ_3 and ϕ_4 indicated in the legend to Figure 2. However, the first four terms will give rise to cross peaks in the 2D spectrum:

$$2N^\epsilon{}_yC^\zeta{}_z \cos^3(2\pi J\tau_d) \rightarrow (\omega_{N\epsilon}, \omega_{H\epsilon})$$

$$2N^{\eta1}{}_yC^\zeta{}_z \cos(2\pi J\tau_d) \sin^2(2\pi J\tau_d) \rightarrow (\omega_{N\eta1}, \omega_{H\epsilon})$$

$$2N^{\eta2}{}_yC^\zeta{}_z \cos(2\pi J\tau_d) \sin^2(2\pi J\tau_d) \rightarrow (\omega_{N\eta2}, \omega_{H\epsilon}) \quad (3)$$

$$8N^\epsilon{}_yC^\zeta{}_zN^{\eta1}{}_yN^{\eta2}{}_y \cos(2\pi J\tau_d) \sin^2(2\pi J\tau_d) \rightarrow (-\omega_{N\eta2} - \omega_{N\eta1} - \omega_{N\epsilon}, \omega_{H\epsilon}), (\omega_{N\eta2} + \omega_{N\eta1} - \omega_{N\epsilon}, \omega_{H\epsilon}), (\omega_{N\eta2} - \omega_{N\eta1} + \omega_{N\epsilon}, \omega_{H\epsilon}), (-\omega_{N\eta2} + \omega_{N\eta1} + \omega_{N\epsilon}, \omega_{H\epsilon})$$

where the appropriate term at point b in the sequence and the cross peak(s) arising from that term are indicated on the left and right hand sides of the arrows, respectively. Note that the intensities of cross peaks at the frequencies indicated in eq 3 are proportional to the square of the trigonometric terms indicated on the left hand side of the arrows. For $2\tau_d \sim 14$ ms, signals of appreciable intensity are obtained for the first three terms. However 3-spin cross peaks arising from magnetization of the form $8N^\epsilon{}_yC^\zeta{}_zN^{\eta1}{}_yN^{\eta2}{}_y$ at point b in the sequence are reduced in intensity by a factor of 4 relative to the cross peaks of interest at $(\omega_{N\eta1},\omega_{H\epsilon})$ and $(\omega_{N\eta2},\omega_{H\epsilon})$. By careful positioning of the ^{15}N carrier in this experiment it is relatively straightforward to distinguish 3-spin peaks from the cross peaks of interest. Equation 3 indicates that, by placing the carrier in the center of the N^ϵ region of the nitrogen spectrum, the triple-spin peaks are well separated from the remaining peaks.

(3) Arg−H$^\eta$(N$^\eta$C$^\zeta$N$^\epsilon$)H$^\epsilon$ (Figure 2c). The flow of magnetization in this pulse scheme is

$$H^\eta(t_1) \xrightarrow{J_{NH}} N^\eta \xrightarrow{J_{N\eta C\zeta}} C^\zeta \xrightarrow{J_{N\epsilon C\zeta}} N^\epsilon \xrightarrow{J_{NH}} H^\epsilon(t_2) \quad (4)$$

with the active couplings listed above the arrows. In this experiment there is net transfer of magnetization from the H^η proton to H^ϵ using heteronuclear cross polarization (CP)[34,35] to effect the transfer. Note that the transfer is asymmetric; that is, magnetization can be transferred from H^η to H^ϵ giving rise to cross peaks at $(\omega_{H\eta},\omega_{H\epsilon})$, but the transfer pathway from H^ϵ to H^η giving rise to cross peaks at $(\omega_{H\epsilon},\omega_{H\eta})$ is not allowed. This asymmetry is due to the choice of the delays, τ_b and τ_c, during which times a ^{15}N spin evolves due to the one-bond coupling with its directly attached proton spin(s). By choosing $2\tau_c = 1/(2J_{NH})$ magnetization which originates on the H^ϵ spin at the start of the experiment and is transferred to transverse N^η magnetization at the end of the heteronuclear CP period evolves during the interval $2\tau_c$ to give a term of the form $4N^\eta{}_{tr}H^{\eta a}{}_zH^{\eta b}{}_z$, where $N^\eta{}_{tr}$ and $H^{\eta a,b}{}_z$ denote transverse N^η magnetization and z magnetization of the two protons attached to N^η. This term is not converted into observable magnetization by the action of the remaining pulses in the sequence. In addition, it is straightforward to show that, while diagonal peaks at $(\omega_{H\epsilon},\omega_{H\epsilon})$ will be observed in spectra, peaks at $(\omega_{H\eta},\omega_{H\eta})$ will not be observed. The absence of these peaks is due to (i) the choice of the delays τ_b $\{1/(8J_{NH})\}$ and τ_c $\{1/(4J_{NH})\}$ as before and (ii) the action of the ^{1}H 90°$_y$ pulse immediately prior to the start of the heteronuclear CP period which effectively acts as a purge pulse by transforming terms which would normally give rise to $(\omega_{H\eta},\omega_{H\eta})$ diagonal peaks into operators corresponding to coherences which are not refocused into observable magnetization by the remaining portion of the sequence. For example,

(33) London, R. E.; Walker, T. E.; Whaley, T. W.; Matwiyoff, N. A. *Org. Magn. Reson.* **1977**, *9*, 598.

(34) Bearden, D. W.; Brown, L. R. *Chem. Phys. Lett.* **1989**, *163*, 432.

(35) Zuiderweg, E. R. P. *J. Magn. Reson.* **1990**, *89*, 533.

in the absence of the purge pulse the following pathway is allowed:

$$\underset{(a)}{H^{\eta 1a}{}_z} \rightarrow \underset{(b)}{H^{\eta 1a}{}_z N^{\eta 1}{}_{tr}} \rightarrow \underset{(c)}{H^{\eta 1a}{}_z N^{\eta 1}{}_{tr}} \rightarrow \underset{(d)}{H^{\eta 1b}{}_z N^{\eta 1}{}_{tr}} \rightarrow \underset{(e)}{H^{\eta 1b}{}_{tr}} \quad (5)$$

where $H^{\eta 1a}{}_z$ is the z component of magnetization from one of the two $\eta 1$ protons (distinguished by the superscripts **a** and **b**), N_{tr} is transverse nitrogen magnetization, and the letters a, b, etc. map the terms to the appropriate positions in the pulse scheme denoted by a, b, etc. Of course, an identical pathway exists for $\eta 2$. Note that, in the scheme of eq 5, the heteronuclear CP period does not serve to transfer magnetization. These paths, therefore, give rise to peaks of the form $(\omega_{H^{\eta 1a}},\omega_{H^{\eta 1b}})$ and $(\omega_{H^{\eta 1b}},\omega_{H^{\eta 1a}})$ as well as peaks arising from the transfer of magnetization within the second NH_2 group. In many cases, these peaks are either on the diagonal or very close to the diagonal. The addition of a ^1H 90°$_y$ purge pulse prior to the start of the CP period creates operators of the form $H^{\eta 1a}{}_x N^{\eta 1}{}_{tr}$ which are eliminated by the action of gradient 5 in Figure 2c and in any event are not refocused into observable signals by the remaining pulses in the sequence. Note that the partial elimination of diagonal or near-diagonal peaks through the use of the purge pulse aids in the observation of cross peaks that connect H^η and H^ϵ protons having similar chemical shifts.

The ^1H 90°$_y$ pulse applied prior to the start of the heteronuclear CP period plays another important role in the elimination of artifacts brought about due to exchange of labile protons (such as H^η or H^ϵ protons) with water magnetization that has a different steady state value depending on whether the cosine-, or sine-modulated t_1 component is recorded. Quadrature components in t_1 are obtained by recording spectra with $\phi_1 = x$ and $\phi_1 = y$ in an interleaved manner. When $\phi_1 = x$, the water magnetization (which is on-resonance) is along the $-y$ axis immediately prior to the heteronuclear CP period and is restored to the $+z$ axis by the effects of radiation damping during this time (64 ms). The remaining pulses in the sequence are of the appropriate phase so that the water magnetization lies along $+z$ prior to detection. In contrast, when $\phi_1 = y$ the water magnetization is along the $+z$ axis prior to the application of this ^1H 90°$_y$ pulse. The action of the pulse rotates the water into the transverse plane where it is restored to the $+z$ axis by radiation damping. At first glance it may seem that this pulse is unnecessary when $\phi_1 = y$ since in its absence the water magnetization is along the $+z$ axis at the end of the CP period in any event. However, as was discussed in the context of the Arg−$H^\epsilon(N^\epsilon C^\delta)H^\delta$ sequence previously, it is essential that equivalent steady state values for the water magnetization be obtained for both $\phi_1 = x$ and $\phi_1 = y$ components. If this is not the case, exchange of labile protons with water will create inequivalent values of the protein magnetization at the start of the sequence for $\phi_1 = x$ and $\phi_1 = y$ leading to quadrature artifacts. Since the CP time may not be sufficient to ensure that water is completely restored to the $+z$ axis via radiation damping for $\phi_1 = x$, we prefer to place the water magnetization in the transverse plane at the start of the CP sequence for both $\phi_1 = x$ and y so that equivalent steady state values of the water magnetization are achieved in a manner independent of the phase ϕ_1. For a CP mixing time of 64 ms employed in the present study, this strategy is superior to other pulse schemes which make use of additional shaped pulses to minimize water saturation and place the water along the $+z$ axis prior to detection. However a limitation of the present approach is that it does require that radiation damping be used to restore the water magnetization to the $+z$ axis and is therefore only applicable for relatively long CP times.

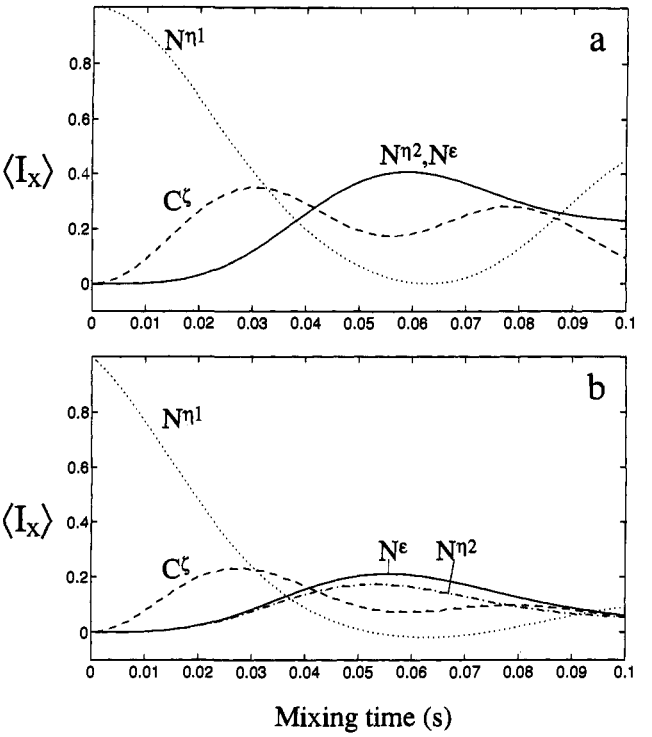

Figure 3. Transfer functions for magnetization exchange from $N^{\eta 1}$ to C^ζ, N^ϵ, and $N^{\eta 2}$ as a function of the transfer time, assuming that (a) all of the spins have equal T_2 values of ∞ or (b) T_2 values of 80, 120, and 60 ms for the C^ζ, N^ϵ, and N^η spins,[23] respectively. An on-resonance spin lock CP field was used for simplicity with $J_{C^\zeta-N} = 20$ Hz.[33] Equal T_1 values of ∞ are assumed for all spins in the simulations. The simulations were performed by assuming a CP Hamiltonian, $\mathscr{H}$, of the form $\mathscr{H} = \pi J_{C-N}[(N^{\eta 1}{}_y C^\zeta{}_y + N^{\eta 1}{}_z C^\zeta{}_z) + (N^{\eta 2}{}_y C^\zeta{}_y + N^{\eta 2}{}_z C^\zeta{}_z) + (N^\epsilon{}_y C^\zeta{}_y + N^\epsilon{}_z C^\zeta{}_z)]$ and by a complete density matrix treatment with the initial condition that at $t = 0$ the only magnetization present is the x component of spin $N^{\eta 1}$. Transverse relaxation was included by solving for the density operator in 1 ms intervals; at the completion of each interval the density matrix is decomposed into its product operator terms, and each operator is allowed to relax at the appropriate rate. The relaxation rate of a product term is assumed to be the sum of the rates of each component operator in the term. The x components of magnetization relax with prescribed T_2 values (see above) while the y and z components relax with rates which are averages of $1/T_1$ and $1/T_2$ rates due to rapid rotation about the spin lock axis (x).

As discussed above the pulse scheme of Figure 2c permits the flow of magnetization from H^η to H^ϵ. It is straightforward to change the magnetization transfer pathway from H^ϵ to H^η by interchanging the delays τ_b and τ_c. However, because the line widths of arginine H^η protons are in general significantly larger than the line widths of H^ϵ protons (see below) and resolution in the Arg−$H^\eta(N^\eta C^\zeta N^\epsilon)H^\epsilon$ spectrum is limited in t_1 by the fairly course digitization employed, spectra of higher resolution can be obtained if the H^η shift is recorded indirectly (t_1) and the H^ϵ shift recorded during the much longer t_2 period.

Figure 3 illustrates the transfer functions for magnetization exchange from $N^{\eta 1}$ to C^ζ, N^ϵ, and $N^{\eta 2}$ as a function of the heteronuclear CP transfer time assuming (a) that all of the spins have equal T_2 values of ∞ or (b) T_2 values of 80, 120, and 60 ms for the C^ζ, N^ϵ, and N^η spins,[23] respectively. A simple continuous wave (CW) spin lock mixing scheme was used in the simulations, and equal C^ζ−N coupling constants of 20 Hz have been assumed.[33]

It is also possible to design an Arg−$H^\eta(N^\eta C^\zeta N^\epsilon)H^\epsilon$ pulse scheme whereby magnetization is transferred from H^η to N^ϵ based on a series of CP transfer steps exclusively. Applications of such a sequence to a sample of the PLCC SH2 domain−

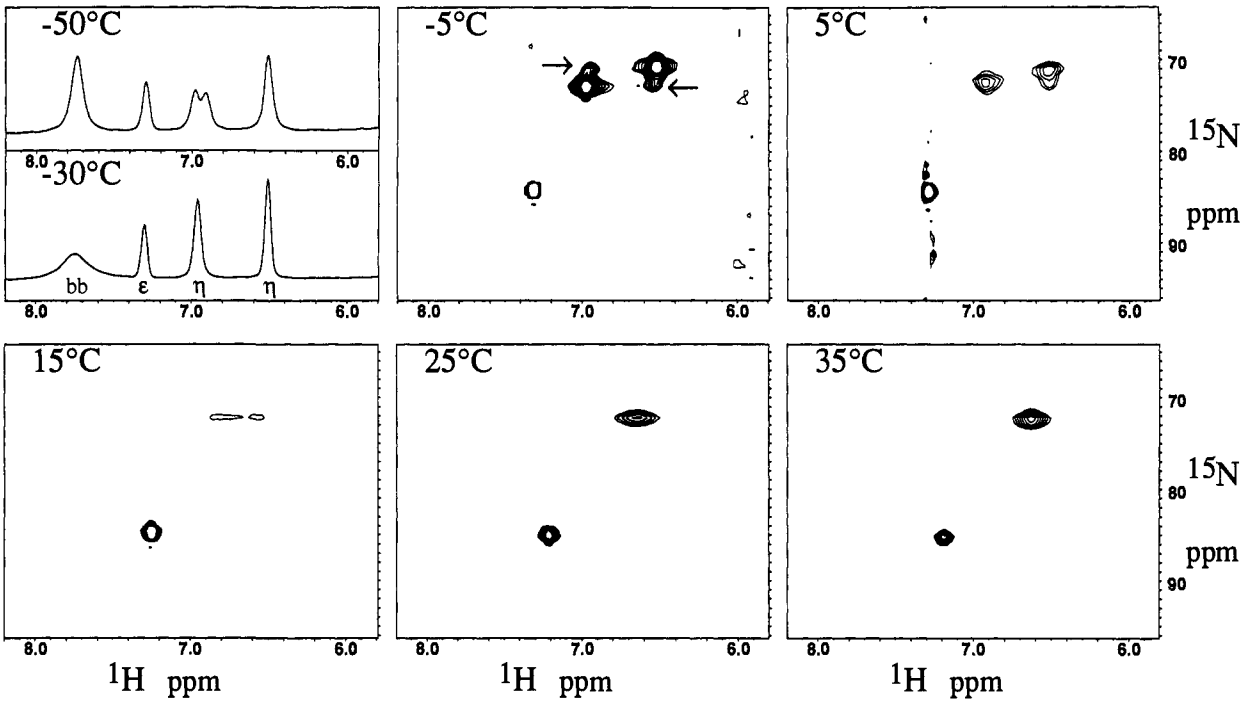

Figure 4. Spectra of the amino acid arginine as a function of temperature. For 1D spectra recorded at −50 °C and −30 °C a sample of 0.35 M natural abundance arginine dissolved in 45% H_2O, 5% D_2O, and 50% methanol was used. Two-dimensional HSQC spectra (temperatures ≥ −5 °C) were recorded on a 0.7 M natural abundance sample in 90% H_2O and 10% D_2O, pH 5.7 (room temperature value). Assignments of the resonances are indicated below the 1D spectrum recorded at −30 °C, where ϵ and η refer to the H^ϵ and H^η protons, respectively, and bb is the backbone HN proton.

pY1021 complex gave results which were similar to the results of the experiment of Figure 2c (see below). In contrast, an Arg−$H^\eta(N^\eta C^\zeta N^\epsilon)H^\epsilon$ sequence with magnetization transfer from N^η to C^ζ and from C^ζ to N^ϵ established via a series of INEPT[20] transfers resulted in spectra of very poor quality. Insight into why the heteronuclear CP pulse scheme is superior to sequences based on INEPT transfers of magnetization can be obtained from Figure 4 which shows the temperature dependence of spectra of a sample of the amino acid arginine. It is clear that, at −50 °C, rotation about one of the C^ζ−N^η bonds is sufficiently slowed so that distinct chemical shifts can be observed for the two H^η protons of one of the NH_2 groups. As the temperature is raised the rotation rate about this C^ζ−N^η bond is increased so that only a single H^η proton chemical shift is observed. However, the HSQC spectrum of arginine recorded at −5 °C shows two distinct (N^η,H^η) "auto" peaks, at 6.52 and 70.78 ppm and at 6.97 and 72.89 ppm, indicating that rotation about the N^ϵ−C^ζ bond is hindered to some extent. It is interesting to note that even at this temperature there are exchange cross peaks (indicated by the arrows in Figure 4) corresponding to the transfer of magnetization from one η site to the other due to rotation about the N^ϵ−C^ζ bond. Numerical simulations show that these exchange peaks arise from exchange events which occur during the t_1 period as well as during the refocusing period of the final INEPT portion of the sequence, which in the present case corresponds to an interval of 4.6 ms. As the temperature is raised the intensities of the (N^η,H^η) auto peaks decrease due to broadening in both the ^1H and ^{15}N dimensions (intermediate exchange regime) to the point where at 15 °C the cross peaks are barely visible. At higher temperatures, rotation about the N^ϵ−C^ζ bond becomes sufficiently rapid so that only a single (N^η,H^η) auto peak is observed. Heteronuclear CP transfer schemes become particularly advantageous relative to their counterparts based on INEPT transfers when the exchange between $\eta 1 \leftrightarrow \eta 2$ occurs at a rate, k, in the regime $\tau^{-1} < k < \Delta\omega$, where 2τ is the time that magnetization evolves in the INEPT scheme prior to transfer and $\Delta\omega$ is the chemical shift difference between $\eta 1$ and $\eta 2$.[36] In the limit that the heteronuclear CP field is very much stronger than the chemical shift offsets of spins $N^{\eta 1}$ and $N^{\eta 2}$ from the carrier, transfer of magnetization via CP is essentially independent of exchange. For the study of arginines in proteins where there is likely to be a range of rotation rates about N^ϵ−C^ζ bonds depending on the particular contacts of a given arginine side chain, the N ↔ C heteronuclear CP scheme described here will be superior to INEPT-based magnetization transfers.

Based on the temperature dependence of the intensity of the (N^η,H^η) auto peaks in Figure 4 it is possible to obtain a qualitative estimate for the $\eta 1 \leftrightarrow \eta 2$ jump rate in arginine at the temperature of maximum broadening, ~15 °C. Assuming that the $^{15}N^\eta$ and $^1H^\eta$ chemical shift differences at −5 °C are essentially independent of exchange, a jump rate of ~500 s^{-1} is estimated at 15 °C. More quantitative estimates of the jump rate vs temperature can be obtained by an experiment in which a mixing time, T_m, is inserted immediately after the final 90° ^{15}N pulse in a regular ^1H−^{15}N HSQC pulse scheme.[20,21] An estimate of the $\eta 1 \leftrightarrow \eta 2$ jump rate, k, can be obtained by quantitating the buildup of cross peaks ($N^{\eta i}$,$H^{\eta j}$) ($i \neq j$) corresponding to magnetization which originates on one of the two NH_2 guanidino groups and is transferred to the second group

(36) Rance, M. NMR Gordon Research Conference, Magnetic Resonance in Medicine and Biology, New England College, July 17−22, 1994.
(37) McCoy, M.; Mueller, L. *J. Am. Chem. Soc.* **1992**, *114*, 2108.
(38) States, D. J.; Haberkorn, R.; Ruben, D. J. *J. Magn. Reson.* **1982**, *48*, 286.
(39) Marion, D.; Ikura, M.; Tschudin, R.; Bax, A. *J. Magn. Reson.* **1989**, *85*, 393.
(40) Shaka, A. J.; Lee, C. J.; Pines, A. *J. Magn. Reson.* **1988**, *77*, 274.
(41) Grzesiek, S.; Bax, A. *J. Biomol. NMR* **1993**, *3*, 185.
(42) Logan, T. M.; Olejniczak, E. T.; Xu, R. X.; Fesik, S. W. *J. Biomol. NMR* **1993**, *3*, 225.
(43) Marion, D.; Kay, L. E.; Sparks, S. W.; Torchia, D. W.; Bax, A. *J. Am. Chem. Soc.* **1989**, *111*, 1515.
(44) Zuiderweg, E. R. P.; Fesik, S. W. *Biochemistry* **1989**, *28*, 2387.

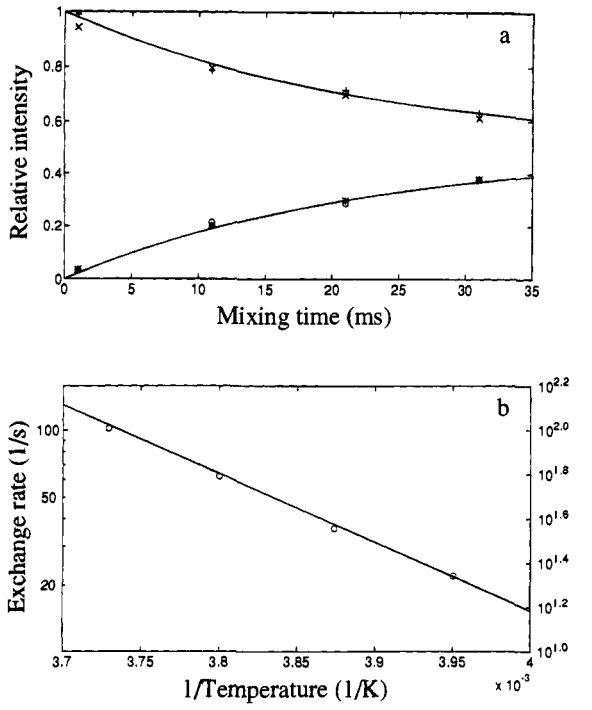

Figure 5. (a) Relative intensity of the auto ($N^{\eta i}$,$H^{\eta i}$) and cross ($N^{\eta i}$,$H^{\eta j}$) ($i \neq j$) peaks as a function of mixing time, T_m, in HSQC-exchange experiments[20,21] recorded on a sample of 0.56 M natural abundance arginine dissolved in 70% H_2O, 10% D_2O, 20% methanol. Auto peak intensities are indicated by the symbols + and ×, cross peak intensities by the symbols o and *. (b) Arrhenius plot of the $\eta 1 \leftrightarrow \eta 2$ jump rate versus temperature from which an activation energy of 14.0 ± 0.2 kcal mol^{-1} is calculated.

during T_m. As described in the methods section, if (i) cross-relaxation during T_m is neglected and (ii) a two-site $\eta 1 \leftrightarrow \eta 2$ jump model with each site having equivalent relaxation properties is assumed,

$$[I_a(T_m) - I_c(T_m)]/[I_a(T_m) + I_c(T_m)] = B \exp(-2kT_m) \quad (6)$$

where $I_c(T_m)$ and $I_a(T_m)$ are the intensities of the cross ($N^{\eta i}$,$H^{\eta j}$) ($i \neq j$) and auto ($N^{\eta i}$,$H^{\eta i}$) peaks, respectively, at a mixing time of T_m. The effects of exchange during the reverse INEPT period are included in the factor B in equation 6. Profiles of $I_c(T_m)$ and $I_a(T_m)$ from $^1H-^{15}N$ exchange spectra of arginine recorded at −20 °C are illustrated in Figure 5a. Note that the decay curves of both auto peaks are the same and that the time dependence of each of the cross peaks are also equivalent. Figure 5b plots the values of k measured as a function of temperature from which an activation energy of 14.0±0.2 kcal mol^{-1} is obtained for rotation about the $N^\epsilon-C^\zeta$ bond.

Figure 6 illustrates the quality of the data obtained from the pulse schemes described in the present paper. The results from the Arg−$H^\epsilon(N^\epsilon C^\delta)H^\delta$, Arg−$H^\epsilon(N^\epsilon C^\zeta)N^\eta$, and Arg−$H^\eta(N^\eta C^\zeta N^\epsilon)$-$H^\epsilon$ experiments are shown in Figure 6a−c, respectively, and the N^η, H^η, N^ϵ, and H^ϵ chemical shifts are summarized in Table 1. In many cases N^η nitrogen and H^η proton chemical shifts are degenerate, consistent with rapid rotation about both $N^\epsilon-C^\zeta$ and $C^\zeta-N^\eta$ bonds. On the other hand, Arg 18 and Arg 39 each show two N^η nitrogens and two H^η protons with distinct chemical shifts. Of significance is the fact that both N^η and all four H^η chemical shifts for Arg 37 are unique, suggesting slow rotation about both $N^\epsilon-C^\zeta$ and $C^\zeta-N^\eta$ bonds in this case. The solution structure of the PLCC SH2 domain in complex with a 12-residue phosphopeptide from the PDGFR places Arg 37 at the base of a deep pocket which binds the phosphotyrosine of the peptide.[15] Both the position of this arginine in the structure and the large downfield chemical shifts of both N^η nitrogens and two of the four H^η protons suggest that one H^η proton from each of the two NH_2 groups forms a hydrogen bond with the phosphate oxygens of the phosphotyrosine of the peptide. Information of this sort is particularly important due to the sparsity of NOEs connecting the guanidino portion of arginine side chains to proximal residues in the protein and due to the complete absence of NOEs linking the phosphate group to its neighbors in the structure.

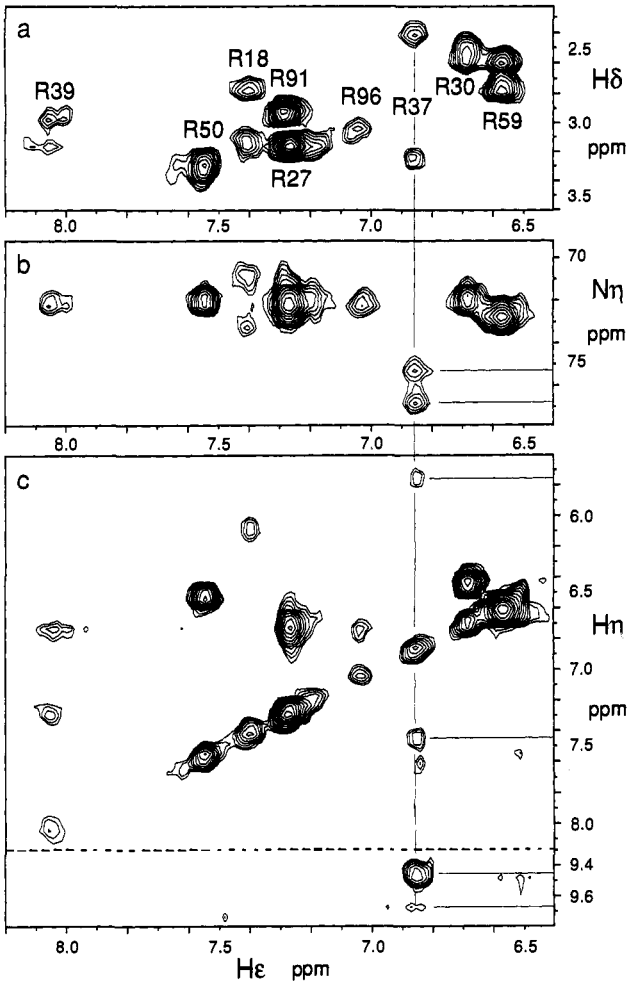

Figure 6. Spectra from the Arg−$H^\epsilon(N^\epsilon C^\delta)H^\delta$ (a), Arg−$H^\epsilon(N^\epsilon C^\zeta)N^\eta$ (b), and Arg−$H^\eta(N^\eta C^\zeta N^\epsilon)H^\epsilon$ (c) experiments.

Table 1. ^{15}N and ^1H Chemical Shifts of Arginine Guanidino Groups in the PLCC−Peptide Complex[a]

residue	$^{15}N^\epsilon$ (ppm)	$^1H^\epsilon$ (ppm)	$^{15}N^\eta$ (ppm)	$^1H^\eta$ (ppm)
Arg 18	86.4	7.40	71.0	6.08
			73.2	*b*
Arg 27	84.8	7.26	72.2	6.73
Arg 30	84.3	6.68	71.9	6.43
Arg 37	81.8	6.86	75.3	5.75, 9.70
			76.8	7.45, 9.45
Arg 39	85.5	8.06	71.9	7.28
			72.2[c]	6.73
Arg 50	86.4	7.54	71.9	6.51
Arg 59	83.6	6.56	72.8	6.62
Arg 91	86.1	7.28	72.2	*d*
Arg 96	85.2	7.03	72.2	6.73

[a] The ^1H chemical shifts are calibrated relative to external TSP, and the ^{15}N chemical shifts are calibrated relative to external liquid NH_3. [b] Not observed due to broadening of the H^η. [c] Confirmed by 3D ^{15}N-edited NOESY[43,44] by observing a cross peak connecting the two H^η. [d] Not observed due to broadening of H^η or overlap with Arg 27 H^η.

In summary, we have described a number of pulse schemes for the assignment of guanidino ^{15}N and ^{1}H chemical shifts based on connectivities established through scalar couplings only. The importance of minimizing saturation of water and of using sequences which are not sensitive to the effects of chemical exchange have been emphasized. The chemical shifts provided by the experiments presented have served as the starting point for understanding and distinguishing the structural roles of individual arginine side chains in the PLCC SH2−phosphopeptide complex. It is likely that the experiments will also find utility in studies of protein−DNA/RNA complexes, where arginine side chains are often involved in crucial interactions bridging the protein and the DNA/RNA.

Acknowledgment. T.Y. and S.M.P. are the recipients of a Human Frontiers Science Program Fellowship and a Medical Research Council of Canada Postdoctoral Fellowship, respectively. We thank Dr. S. Shoelson, Harvard University, for the gift of phosphotyrosine peptide and Dr. Tony Pawson, Mount Sinai Hospital, Toronto, for his enthusiastic support of the research. This work was supported through grants from the Natural Sciences and Engineering Research Council of Canada (L.E.K.), the National Cancer Institute of Canada with funds from the Canadian Cancer Society J.D.F.-K. and L.E.K.), and the Medical Research Council of Canada (J.D.F.-K. and L.E.K.).

JA9438728